

Zero-Shot Calibration of Fisheye Cameras

Jae-Yeong Lee

Electronics and Telecommunications Research Institute (ETRI)

Daejeon 34129, South Korea

jylee@etri.re.kr

Abstract

In this paper, I present a novel zero-shot camera calibration method that estimates camera parameters with no calibration image. It is common sense that we need at least one or more pattern images for camera calibration. However, the proposed method estimates camera parameters from the horizontal and vertical field of view information of the camera without any image acquisition. The proposed method is particularly useful for wide-angle or fisheye cameras that have large image distortion. Image distortion is modeled in the way fisheye lenses are designed and estimated based on the square pixel assumption of the image sensors. The calibration accuracy of the proposed method is evaluated on eight different commercial cameras qualitatively and quantitatively, and compared with conventional calibration methods. The experimental results show that the calibration accuracy of the zero-shot method is comparable to conventional full calibration results. The method can be used as a practical alternative in real applications where individual calibration is difficult or impractical, and in most field applications where calibration accuracy is less critical. Moreover, the estimated camera parameters by the method can also be used to provide proper initialization of any existing calibration methods, making them to converge more stably and avoid local minima.

1. Introduction

Camera calibration is an essential and preliminary step in computer vision. In 3D vision applications, the camera parameters are used to interpret and recover imaging geometry of a camera from a 3D scene to a 2D image. In 2.5D vision applications like visual surveillance, camera calibration is required to normalize and eliminate the influence of the camera-specific parameters on the execution of the algorithm.

In general, camera calibration requires careful acquisition of dozens of pattern images and is usually performed in a desktop environment. However, in real applications,

image acquisition for camera calibration is not an easy problem and can be challenging depending on the circumstances. To calibrate a camera, we usually need to take a number of images of special calibration patterns such as checkerboard, circles, or a known 3D object. The captured pattern images are then used to extract control points which constrain camera parameters and thus they have to be carefully taken such that the patterns do not deviate from the camera's field of view and as many as possible in various positions and angles [6]. This image acquisition process is time-consuming and often challenging especially when a camera is placed on unconstrained areas or fixed in high on the environment like most CCTV cameras. Recent intelligent vision systems usually utilize dozens or hundreds of cameras in one site and therefore camera calibration have become one of the most challenging process in such a field.

There have been lots of approaches to minimize the effort required to acquire images in the literature, namely few-shot calibration approaches. They can be classified into several groups. Most of them use orthogonal pairs of vanishing points in a natural scene or artificial objects [3, 8, 12, 13], or estimate planar homography and then extract camera parameters from the estimated homography [5, 9, 17, 20, 26, 29], or estimate camera parameters using a specially designed 2D or 3D object [7, 10]. These few-shot approaches are more preferred in practical applications because the conventional checkerboard-based calibration requires a lot of images taken with care. However, these simplified few-shot methods still require image acquisition together with a subsequent sophisticated image analysis process. What is worse is that they usually assume zero-distortion of the camera lens or simply ignore the image distortion, which is not the case for most recent wide-angle or fisheye cameras. In these days, more and more cameras are used in real life applications and they tends to use wide-angle lenses to secure a large field of views.

More recently lots of auto calibration approaches based on deep neural network [4, 15, 16, 23, 24, 25, 28] have also been studied. However, these approaches mainly focus on the rectification of the image and their performance still rely

on the acquired images.

In this paper, I adopt a completely different direction and suggest a novel calibration method that estimates camera parameters without any image acquisition, namely *zero-shot* camera calibration method. The method estimates camera parameters by utilizing only the camera specification information without any image acquisition. Since the proposed method does not require image acquisition, no subsequent image analysis nor feature detection which can be oftentimes erroneous is required. The experimental results on eight commercial cameras show that the proposed zero-shot calibration method is able to estimate their camera parameters effectively with an accuracy comparable to conventional image-based calibration methods.

The proposed method is particularly useful for wide-angle or fisheye cameras that have large image distortion. The image distortion of camera lens is modeled in the way fisheye lenses are designed and estimated based on the square pixel assumption of the image sensors. And the experimental result on real cameras shows that the zero-shot method yields better rectification results than a standard calibration method [27].

My work, to the best of my knowledge, is the first one to estimate camera parameters of fisheye cameras without image acquisition. The benefit of the proposed method is obvious and it can be used in various ways. It can be used as a practical alternative in real applications where individual calibration is difficult or impractical, and in most field applications where calibration accuracy is less critical. Moreover, the estimated camera parameters by the zero-shot method can also be used to provide proper initialization of any existing calibration methods, making them to converge more stably and avoid local minima. The effectiveness of this kind of initialization is also demonstrated in the experiment.

The paper is organized as follows. Section 2 describes the proposed camera calibration method along with motivations and technical details. In Section 3, experimental results on real cameras are presented. In the experiment, calibration accuracy is evaluated in terms of RMS pixel re-projection error and compared with conventional calibration methods. In Section 4, a single-shot extension of the method is presented and evaluated. Finally, I conclude the paper with a brief discussion in Section 5.

2. Zero-Shot Calibration Method

2.1. Simplified camera model

In this paper, a simplified pinhole camera projection model is employed where a camera is assumed to have zero skew and unit aspect ratio (square pixels). This assumption naturally holds for most modern cameras because pixel aspect ratios of photodiode cells of modern image sensors are

typically one (square pixel) and also pixel skew is zero or safely negligible. The camera model is further assumed to have zero decentering distortion and the principal point to coincide with the image center.

$$f = f_x = f_y \quad (1)$$

$$c_x = W/2 \quad (2)$$

$$c_y = H/2 \quad (3)$$

where W is the image width and H the image height.

The *square pixel* assumption on the image sensors of modern cameras is the most important premise that the proposed method is based on and motivated from. The physical focal length of a camera is the distance from the lens center to the image sensor when the image is best in focus. In computer vision, however, the focal length as a camera parameter is defined relatively in pixel unit as the ratio of physical focal length to the cell size of the image sensor. More specifically the ratio of the physical focal length to the image sensor cell size in the horizontal direction is defined by f_x and the ratio to the image sensor cell size in the vertical direction is defined by f_y . Therefore, we can naturally assume that f_x and f_y have the same value for most modern cameras where image sensor cells are designed to have square size and arrayed in uniform grids.

2.2. Inconsistency in focal length estimation

The perspective projection of a pinhole camera is described by the following formula [11]

$$r = f \tan \theta \quad (4)$$

where θ is the angle between the principal axis and the incoming ray, r is the distance between the image point and the principal point and f is the focal length.

If a camera follows the perspective projection model, the horizontal and vertical focal length of the camera can be computed directly from its horizontal and vertical field of view angles as follows:

$$\tilde{f}_x = \frac{W/2}{\tan(\theta_h/2)} \quad (5)$$

$$\tilde{f}_y = \frac{H/2}{\tan(\theta_v/2)} \quad (6)$$

where θ_h is horizontal field of view angle and θ_v vertical field of view angle of camera and W is the image width and H the image height. The field of view angles information of a camera are usually given in camera specification which is provided by the manufacturer.

The computed horizontal focal length \tilde{f}_x and vertical focal length \tilde{f}_y should have virtually the same or similar values if the camera follows the *square pixel* assumption. And this property holds in most normal cameras that have little

or no image distortion. For example, Logitech C922 web camera has a horizontal viewing angle of 70.42° and a vertical viewing angle of 43.3° and gives nearly the same value of focal lengths with 720p image as follows.

$$\tilde{f}_x = \frac{1280/2}{\tan(70.42^\circ/2)} = 906.9217 \quad (7)$$

$$\tilde{f}_y = \frac{720/2}{\tan(43.4^\circ/2)} = 906.9431 \quad (8)$$

However, the above conversion is hardly applicable to wide-angle or fisheye cameras. Fisheye cameras have large image distortion and the geometrical relationship in (4) no longer holds. For example, AXIS M2026-LE security camera has a horizontal viewing angle of 130° and a vertical viewing angle of 73° , and gives very different focal length estimates with 720p image as follows.

$$\tilde{f}_x = \frac{1280/2}{\tan(130^\circ/2)} = 298.4369 \quad (9)$$

$$\tilde{f}_y = \frac{720/2}{\tan(73^\circ/2)} = 486.5121 \quad (10)$$

This large difference between \tilde{f}_x and \tilde{f}_y of wide-angle cameras obviously goes against the *square pixel* premise.

2.3. Proposed calibration method

The reason why different \tilde{f}_x and \tilde{f}_y are obtained for wide-angle cameras as above is that \tilde{f}_x and \tilde{f}_y are calculated based on the distorted image size, not the original undistorted image size.

$$\tilde{f}_x = f_{x\text{ distorted}} = \frac{W_{\text{distorted}}/2}{\tan(\theta_h/2)} \quad (11)$$

$$\tilde{f}_y = f_{y\text{ distorted}} = \frac{H_{\text{distorted}}/2}{\tan(\theta_v/2)} \quad (12)$$

The image distortion of a wide-angle camera is dominated by radial distortion. The radial distortion depends only on the distance from the principal point and the further away from the principal point, the more the image is distorted or compressed as shown in Figure 1. Therefore, due to the characteristics of an image whose horizontal resolution is larger than vertical resolution, the more image compression occurs in the horizontal direction. As a result, $f_{x\text{ distorted}}$ becomes smaller than $f_{y\text{ distorted}}$, and this difference becomes larger as the distortion increases.

Let \mathcal{G} be a mapping function that models the radial distortion of an image, ω be model parameter of \mathcal{G} , r_d be the distance from the principal point in *distorted* image, and r_u be the corresponding rectified distance in *undistorted* image.

$$r_d = \mathcal{G}_\omega(r_u) \quad (13)$$

$$r_u = \mathcal{G}_\omega^{-1}(r_d) \quad (14)$$

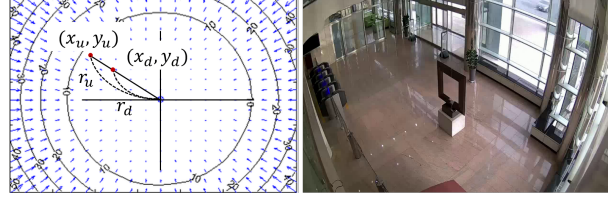


Figure 1. An example of radial distortion distribution (left) and a sample image (right).

Then, the transformation between the field of view angles and focal lengths can be reformulated as follows.

$$f_{x\text{ undistorted}} = \frac{\mathcal{G}_\omega^{-1}(W_{\text{distorted}}/2)}{\tan(\theta_h/2)} \quad (15)$$

$$f_{y\text{ undistorted}} = \frac{\mathcal{G}_\omega^{-1}(H_{\text{distorted}}/2)}{\tan(\theta_v/2)} \quad (16)$$

And the distortion parameter ω can be estimated to minimize the difference between the computed horizontal and vertical focal lengths based on the *square pixel* assumption.

$$\omega^* = \arg \min_{\omega} |f_{x\text{ undistorted}} - f_{y\text{ undistorted}}| \quad (17)$$

Finally, distortion-corrected focal lengths are then obtained with the estimated ω^* as follows.

$$f_x^* = \frac{\mathcal{G}_{\omega^*}^{-1}(W_{\text{distorted}}/2)}{\tan(\theta_h/2)} \quad (18)$$

$$f_y^* = \frac{\mathcal{G}_{\omega^*}^{-1}(H_{\text{distorted}}/2)}{\tan(\theta_v/2)} \quad (19)$$

2.4. Modeling of radial distortion

Radial distortion of image of wide-angle or fisheye cameras can be explained by fisheye lens projection. Unfortunately, however, there is no single fisheye lens projection, but instead fisheye lenses are usually designed to obey one of the following projections [11, 19, 22]:

$$r = 2f \tan(\theta/2) \quad (\text{stereographic}) \quad (20)$$

$$r = f\theta \quad (\text{equidistance}) \quad (21)$$

$$r = 2f \sin(\theta/2) \quad (\text{equisolid angle}) \quad (22)$$

$$r = f \sin(\theta) \quad (\text{orthographic}) \quad (23)$$

where θ is the angle between the principal axis and the incoming ray, r is the distance between the image point and the principal point and f is the focal length.

Radial distortion of wide-angle cameras may be modeled by one of the above projection models. However, it is known that the equidistance projection and equisolid angle projection are most common in real fisheye lenses and stereographic and orthographic models are relatively rare [2, 19].

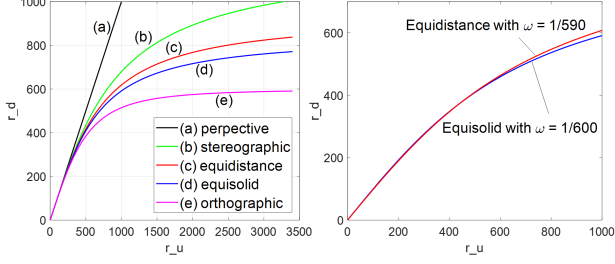


Figure 2. (Left) Graphs of radial distortion mapping of fisheye projection models with $\omega = 1/600$. (Right) Approximation of equisolid angle projection by equidistance projection.

In this work, I adopt the equidistance projection model as the default distortion model considering its simplicity and popularity. However, other projection models can also be adopted depending on the specific camera lenses.

Based on equidistance projection model and from (4) and (21), the radial distortion mapping is formulated as follows.

$$r_d = f \arctan\left(\frac{1}{f} r_u\right) \quad (24)$$

$$r_u = f \tan\left(\frac{1}{f} r_d\right) \quad (25)$$

And, by defining $\omega = 1/f$ be an adjustable distortion parameter, we can reformulate radial distortion mapping \mathcal{G} for equidistance projection model as follows.

$$\mathcal{G}_\omega(r_u) = \frac{1}{\omega} \arctan(\omega r_u) \quad (26)$$

$$\mathcal{G}_\omega^{-1}(r_d) = \frac{1}{\omega} \tan(\omega r_d) \quad (27)$$

Figure 2(Left) shows a graph of the equidistance radial distortion mapping \mathcal{G}_ω along with graphs of other fisheye projection models with $\omega = 1/600$. In the figure, we can see that the two common projection model (*equidistance* and *equisolid angle*) have similar mapping graph and thus they can be approximated by each other with minor error as illustrated in Figure 2(Right). That means the adopted mapping function \mathcal{G}_ω can be applied effectively to model most fisheye and wide-angle camera lenses.

2.5. Implementation

With the specified distortion model \mathcal{G}_ω , the proposed parameter estimation problem is simplified as

$$\omega^* = \arg \min_{\omega} \left| \frac{\tan(\omega W/2)}{\omega \tan(\theta_h/2)} - \frac{\tan(\omega H/2)}{\omega \tan(\theta_v/2)} \right| \quad (28)$$

$$f_x^* = \frac{\tan(\omega^* W/2)}{\omega^* \tan(\theta_h/2)} \quad (29)$$

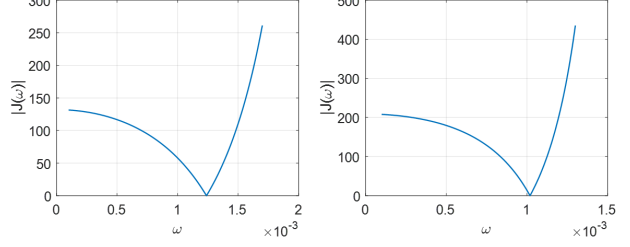


Figure 3. Graphs of $|J(\omega)|$ on two real cameras (left: L6013R, right: Hero9(W1)).

$$f_y^* = \frac{\tan(\omega^* H/2)}{\omega^* \tan(\theta_v/2)} \quad (30)$$

where $W = W_{distorted}$ is image width and $H = H_{distorted}$ image height and θ_h is horizontal field of view angle and θ_v vertical field of view angle.

The estimation of the parameters is nearly straightforward but one caution is required. Let J be the difference between the horizontal and vertical focal lengths.

$$J(\omega) = \frac{\tan(\omega W/2)}{\omega \tan(\theta_h/2)} - \frac{\tan(\omega H/2)}{\omega \tan(\theta_v/2)} \quad (31)$$

such that

$$\omega^* = \arg \min_{\omega} |J(\omega)|. \quad (32)$$

As shown in Figure 3, the graphs of $|J(\omega)|$ plotted for real cameras show that there is a clear solution for (32). Therefore, the distortion parameter ω would be estimated by finding a solution of $J(\omega) = 0$ by Newton-Raphson method [21], for $\omega \geq 0$. However, direct application of Newton-Raphson method is unstable and easy to diverge because the second derivative of $J(\omega)$ is too high (more than 8 orders of magnitude). One solution is to reformulate J so that the numerators and denominators have similar order of values. Newton-Raphson iteration with the following reformulation of J always gives a stable solution and it usually converges within 30 iterations.

$$\omega_{k+1} = \omega_k - \gamma \frac{J_{stable}(\omega)}{\partial J_{stable}(\omega)/\partial \omega} \quad (33)$$

$$J_{stable}(\omega) = \frac{\tan(\theta_v/2)}{\tan(\theta_h/2)} - \frac{\tan(\omega H/2)}{\tan(\omega W/2)} \quad (34)$$

with $\omega_0 = 0.0001$ and learning rate $\gamma = 0.1$.

3. Experiments

In the experiment, the proposed zero-shot calibration method is evaluated qualitatively and quantitatively on 8 commercial cameras with 11 different camera settings. And all the experiment were conducted based on the following experimental setting.



(a) Original Image

(b) Proposed (ZS)

(c) Zhang

Figure 4. Examples of rectification result of test camera images by the proposed method and Zhang’s method [27]. (b) Rectified image of (a) by proposed zero-shot calibration with camera specification only. (c) Rectified image of (a) by Zhang’s method [27] with full calibration using dozens of checkerboard images. From top to bottom: L6013R₁, L6013R₂, Hero9(W1), and Hero9(W2).

Test Cameras. In the experiment, 8 different commercial cameras were used. The experimental settings of the test cameras and their field of view specifications are shown in Table 1. The C905 and C922 are webcams, Hero9 is an action camera, and SNP-6321, L6013R₁, L6013R₂, M2025-LE, M2026-LE are surveillance cameras. The L6013R₁ and L6013R₂ are two cameras of same model. The Hero9’s are physically the same camera but tested with four different digital lens settings (N: narrow, L: linear, W1, W2: wide mode). In the Table, as an exception, the vertical field of view angle of C905 is not specified because only the horizontal field of view angle is provided from the manufacturer’s specification. And it should also be noted that for the M2025-LE, M2026-LE, only the specification information were used without the actual camera.

Calibration and Evaluation Dataset. Dozens of images (from 20 to 49) per test camera were taken carefully us-

ing a calibration checkerboard. For the M2025-LE, M2026-LE, sample images obtained from the manufacturer’s Website were used instead. The captured checkerboard images were used to estimate intrinsic parameters of the test cameras and also to evaluate accuracy of the calibration methods.

Baseline Calibration Methods. The proposed zero-shot calibration method (ZS) was compared with two standard calibration methods of Zhang [27] and a self-implemented fisheye calibration method (FC_{eq.d.}). Zhang [27] is the most common calibration method and is based on polynomial distortion model. The OpenCV [1] implementation of Zhang was used in the experiment. The second baseline method (FC_{eq.d.}) modeled image distortion by *equidistance* fisheye projection model described in (26) and (27) and can be viewed as a full calibration extension of the zero-shot method. I implemented FC_{eq.d.} so that it estimates param-

Camera	Specification				Perspective Projection				Proposed (ZS)			f_{gt}
	W	H	θ_h	θ_v	\tilde{f}_x	\tilde{f}_y	\tilde{f}	\tilde{f}_{err}	ω^*	f^*	f_{err}^*	
C905	1280	720	63.1	-	1042.3	-	1042.3	1.9%	0	1042.3	1.9%	1062.3
C922	1280	720	70.42	43.3	906.9	906.9	906.9	5.3%	0	907.0	5.2%	957.2
Hero9(N)	1920	1080	73	45	1297.4	1303.7	1300.6	0.9%	0.000152	1306.6	1.4%	1288.8
Hero9(L)	1920	1080	92	61	927.1	916.7	921.9	0.7%	0	921.9	0.7%	915.8
SNP-6321	1280	720	62.8	36.8	1048.5	1082.2	1065.4	4.2%	0.000570	1097.7	1.3%	1112.2
Average								2.6%			2.1%	
L6013R ₁	1280	720	86.5	47.8	680.3	812.4	746.4	17.7%	0.001239	870.9	4.0%	907.2
L6013R ₂	1280	720	86.5	47.8	680.3	812.4	746.4	17.7%	0.001239	870.9	4.0%	906.9
Hero9(W1)	1920	1080	118	69	576.8	785.7	681.3	22.0%	0.001019	876.0	0.3%	873.6
Hero9(W2)	1920	1440	122	94	532.1	671.4	601.8	27.9%	0.001051	837.8	0.4%	834.5
M2025-LE	1280	720	115	64	407.7	576.1	491.9	19.9%	0.001589	648.8	5.7%	613.9
M2026-LE	1280	720	130	73	298.4	486.5	392.5	35.4%	0.001775	568.8	6.3%	607.1
Average								23.4%			3.5%	

Table 1. Error evaluation of the estimated focal lengths of the perspective projection and proposed zero-shot method.

ters so as to minimize the sum of pixel reprojection errors by using the Levenberg-Marquardt algorithm [18].

3.1. Qualitative evaluation

In the first experiment, I evaluate the quality of the camera parameters estimated with the proposed zero-shot calibration method. The estimated distortion parameters (ω^*) and focal lengths (f^*) for the 11 test cameras are shown in Table 1.

Quality of Distortion Parameter. The quality of the estimated distortion parameters is evaluated by comparing the rectification results of the test camera images.

Figure 4 shows rectification result of sample images of test cameras by the proposed method and Zhang’s method [27]. As we can see that, the images are surprisingly well rectified by the proposed method although only the camera specifications were used. And also, the results are shown to be better than those of Zhang’s method [27], where the camera parameters were estimated by full calibration using dozens of the checkerboard images.

As another example, Figure 5 shows sample rectification results of internet images with their camera specification by the proposed zero-shot calibration method. The cameras are those that I don’t really have, and thus test sample images were obtained from the manufacturer’s Website. The results also show that the images are well rectified up to image corners.

Quality of Focal Length. The estimated focal lengths are evaluated by the following deviation error measure.

$$f_{err} = \frac{|f - f_{gt}|}{f_{gt}} \quad (35)$$

where f is the estimate focal length and f_{gt} is ground truth value. Since actual ground truth is unknown, focal lengths



Figure 5. Sample rectification results of internet images with their camera specification by proposed zero-shot calibration method. The cameras are M2025-LE and M2026-LE from top to bottom.

obtained from full calibration of Zhang’s method [27] were used as a ground truth instead. In cases of M2025-LE and M2026-LE, only the specification information were used without real cameras and their ground truth focal lengths were manually estimated with internet image samples using the method of Košecká and Zhang [12].

The evaluated focal length errors for perspective projection and proposed method are shown in Table 1, where the cameras are sorted in two groups so that the narrow-angle cameras are listed at the top and wide-angle cameras listed down. First, the estimated focal lengths by perspective projection are shown by \tilde{f}_x and \tilde{f}_y in Table 1. As previously described, they show large difference for wide-angle cameras while similar for narrow-angle cameras. And their averaged value \tilde{f} are shown to give large deviation error from the ground truth of an average of 23.4%. We can see that the deviation error for perspective projection increases roughly proportional to the field of view angles of the camera. The

	N	Pers. ϵ	ZS ϵ	Zhang ϵ	FC _{eq.d.} ϵ
C905	20	0.98	0.98	0.49	0.71
C922	22	1.18	1.18	0.32	0.51
Hero9(N)	22	0.78	0.91	0.53	0.57
Hero9(L)	25	1.00	1.00	0.43	0.50
SNP-6321	30	2.59	0.69	0.37	0.49
Average	23.8	1.31	0.95	0.43	0.55
L6013R ₁	49	15.50	2.15	0.69	1.03
L6013R ₂	23	14.32	1.50	0.40	0.51
Hero9(W1)	30	37.78	0.48	1.04	0.47
Hero9(W2)	29	45.01	0.76	1.16	0.75
Average	32.8	28.15	1.22	0.82	0.69

Table 2. The RMS reprojection error in pixels.

high deviation error of perspective projection is because it does not reflect the image distortion of a camera. On the other hand, the proposed zero-shot method estimates distortion parameters (ω) directly from the camera specification and then estimates distortion-corrected focal lengths, giving more accurate estimate. The results in Table 1 show that by applying the proposed zero-shot method the deviation errors were greatly reduced from 23.4% to 3.5% on average for wide-angle cameras. As for narrow-angle cameras, the error also slightly decreased from 2.6% to 2.1%.

3.2. Quantitative evaluation

In the second experiment, I evaluate accuracy of the proposed method in terms of pixel reprojection error.

Let N calibration images was obtained for a camera and let each calibration image have M control points. And let p_{ij} be the measured j -th control point of i -the calibration image and $\tilde{p}_{ij} = K[R_i|t_i]P_{ij}$ be the projected control point using the estimated camera parameters of the camera, where K is estimated camera parameter, R_i and t_i are the external camera parameters of i -th calibration image, and P_{ij} is the world coordinate of the control point. The external camera parameters were estimated for each calibration image from the correspondences between $K^{-1}p_{ij}$ and P_{ij} using the PnP algorithm [14]. Then the root mean square (RMS) pixel reprojection error ϵ is computed as follows.

$$\epsilon^2 = \frac{1}{NM} \sum_{i=1}^N \sum_{j=1}^M \|p_{ij} - \tilde{p}_{ij}\|^2 \quad (36)$$

In the experiment, I first estimated camera parameters of 9 cameras from their specifications using the proposed method, and then computed the RMS reprojection errors using the estimated camera parameters on the test images set. The result is shown in Table 2.

The proposed approach is shown to give an average of 1.22 RMS error for wide-angle cameras despite using only

camera specification information. And this result is quite comparable to Zhang [27], which had performed full optimization on the evaluation images and gave 0.82 RMS error on average. As for narrow-angle cameras, the proposed method (ZS) gave 0.95 RMS error and Zhang gave 0.43 RMS error on average.

For the reference, results using other calibration methods are also presented in Table 2. As expected, the simple perspective projection estimation (Pers.) gave the most high RMS error of 28.15 on average for wide-angle cameras but an average of 1.31 RMS error for narrow-angle cameras. As for fisheye calibration method (FC_{eq.d.}), it gave an average of 0.69 RMS error for wide-angle cameras, which is better than Zhang. However, Zhang is shown to give better result than FC_{eq.d.} for narrow-angle cameras.

4. Application to Single-Shot Calibration

The primary purpose of the proposed method is to calibrate cameras without any image acquisition nor image processing. However, it can easily be extended as a single-shot or few-shot approach. The method to extend is to first find the initial parameters with the zero-shot method and then refine them on calibration images. The estimated initial parameters can also be used to provide proper initialization of any existing calibration methods.

An additional experiment was conducted to evaluate the effectiveness of this single-shot application. Here, the calibration is performed with only one calibration image. And then the estimated parameters are evaluated over all calibration images, giving a generalization error. In order to evaluate single-shot calibration methods properly, I defined two error metric. One is fitting RMS error and the other is generalization RMS error. For a given single-shot calibration method and a test camera with N calibration images, an *average generalization error* ($\bar{\epsilon}_{gen}$) and *average fitting error* ($\bar{\epsilon}_{fit}$) are computed as follows.

$$\bar{\epsilon}_{gen} = \frac{1}{N} \sum_{k=1}^N \sqrt{\frac{1}{NM} \sum_{i=1}^N \sum_{j=1}^M \|p_{ij} - \tilde{p}_{ij}^{(k)}\|^2} \quad (37)$$

$$\bar{\epsilon}_{fit} = \frac{1}{N} \sum_{k=1}^N \sqrt{\frac{1}{M} \sum_{j=1}^M \|p_{ij} - \tilde{p}_{ij}^{(k)}\|^2} \quad (38)$$

where $\tilde{p}_{ij}^{(k)}$ is the projected control point using the single-shot calibration result which have calibrated on k -th calibration image only. Note that the *single-shot* calibration is performed for each image and then the evaluation results are averaged.

The evaluation results are shown in Table 3. First, the single-shot fisheye calibration (FC_{eq.d.}⁽¹⁾) is shown to give 9.22 RMS generalization error and 6.54 RMS fitting error

	N	$FC_{eq.d.}^{(1)}$	$Zhang^{(1)}$	ZS	$FC_{eq.d.}^{(1)} + ZS$	$Zhang^{(N)}$
		$\bar{\epsilon}_{gen} (\bar{\epsilon}_{fit})$	$\bar{\epsilon}_{gen} (\bar{\epsilon}_{fit})$	ϵ	$\bar{\epsilon}_{gen} (\bar{\epsilon}_{fit})$	ϵ
C905	20	6.48 (5.35)	1.06 (0.35)	0.98	0.89 (0.64)	0.49
C922	22	3.49 (3.03)	0.52 (0.17)	1.18	0.98 (0.84)	0.32
Hero9(N)	22	3.67 (3.34)	0.77 (0.46)	0.91	0.68 (0.59)	0.53
Hero9(L)	25	5.80 (5.43)	0.67 (0.37)	1.00	0.97 (0.74)	0.43
SNP-6321	30	4.96 (3.80)	1.08 (0.23)	0.69	0.59 (0.41)	0.37
Average	23.8	4.88 (4.19)	0.82 (0.32)	0.95	0.82 (0.64)	0.43
L6013R ₁	49	4.20 (2.20)	0.90 (0.26)	1.50	0.88 (0.68)	0.69
L6013R ₂	23	6.26 (2.65)	2.21 (0.39)	2.15	1.54 (1.13)	0.40
Hero9(W1)	30	10.87 (7.36)	3.41 (0.56)	0.48	0.53 (0.44)	1.04
Hero9(W2)	29	15.55 (13.95)	2.22 (0.69)	0.76	0.81 (0.70)	1.16
Average	32.8	9.22 (6.54)	2.19 (0.48)	1.22	0.94 (0.73)	0.82

Table 3. Evaluation result of single-shot calibration. N denotes the number of images obtained for each test camera.

on average for wide-angle cameras (the superscripted numbers in the method name denote the number of images used for calibration). Zhang⁽¹⁾ gave better result of 2.19 RMS generalization error with 0.48 RMS fitting error for wide-angle cameras on average but it is still worse than the zero-shot result of 1.22 RMS error.

Those results imply that the single-shot calibration methods are easy to fail or overfit the image, giving high generalization error. However, if we combine single-shot calibration with the proposed zero-shot calibration (ZS) such that ZS provides initial estimates of the parameters, we can expect that the methods converge more stably or avoid local minima. The experimental result in Table 3 shows that with the combination of $FC_{eq.d.}^{(1)}$ and ZS, the RMS generalization error was greatly reduced from 9.22 to 0.94 for wide-angle cameras, justifying the effectiveness of this application. The combined calibration method is still a single-shot method but its performance was comparable to Zhang’s full calibration result (Zhang^(N)) which gave 0.82 RMS error.

5. Discussion and Conclusion

In this paper, I presented a novel zero-shot calibration method that estimates camera parameters with no calibration image. The experimental results on eight commercial cameras showed that the proposed method was able to estimate their camera parameters effectively with an accuracy comparable to conventional image-based calibration method. Moreover, the estimated camera parameters by the method can also be used to provide proper initialization of any existing calibration methods, and the effectiveness of this kind of initialization was also demonstrated in the experiment.

Applications. My work is the first one to estimate camera parameters of fisheye cameras without image acquisition and it is expected to be practically utilized in various applications. For example, it can be used as a practical al-

ternative in field applications where individual calibration is difficult or infeasible, and in most visual surveillance applications where calibration accuracy is less critical.

Adaptive Selection of Fisheye Model. In this paper, I adopted an equidistance fisheye projection model as our default distortion model. It is expected to work for most cases but it can be sometime problematic when a camera deviates from the model. One solution is to select distortion model adaptively depending on the cameras. The suggested zero-shot method can be extended to select distortion model adaptively if a diagonal field of view angle is additionally available. The horizontal, vertical, and diagonal view angles give three constraints on the radial mapping and then a model that best meets these constraints can be selected.

Limitations. My approach has several limitations. First, it cannot be applied for the cameras that their specification are not provided. And the cameras that have wide-range varifocal lenses are also not applicable. The propose method is particularly useful for fisheye cameras that have large image distortion but it’s not very useful for narrow-angle cameras. However, even a narrow-angle camera, it can be effectively utilized when the camera has image distortion.

Future Works. One future work is to evaluate the influence of camera auto-focusing and the accuracy of the field of view angles provided by the manufacturers. Another work is to combine the method with more conventional calibration methods and evaluate their effectiveness. Quantitative comparison with recent deep learning-based approaches on benchmark data set is also another work. Last one is to compare the influence of fisheye projection model selection on the performance on real cameras and to extend the method to select distortion model adaptively.

Acknowledgement

This work was supported by the ICT R&D program of MSIT/IITP. [2019-0-01309, Development of AI Technology for Guidance of a Mobile Robot to its Goal with Uncertain Maps in Indoor/Outdoor Environments]

References

- [1] OpenCV. <https://opencv.org/>. 5
- [2] B. Akins. Field of View - Rectilinear and Fisheye lenses. http://www.bobatkins.com/photography/technical/field_of_view.html. 3
- [3] Paul Beardsley and David Murray. Camera calibration using vanishing points. In *BMVC92*, pages 416–425. Springer, 1992. 1
- [4] C. Chao, P. Hsu, H. Lee, and Y. F. Wang. Self-Supervised Deep Learning for Fisheye Image Rectification. In *ICASSP 2020 - 2020 IEEE International Conference on Acoustics, Speech and Signal Processing (ICASSP)*, pages 2248–2252, May 2020. ISSN: 2379-190X. 1
- [5] Zhou Chuan, Tan Da Long, Zhu Feng, and Dong Zai Li. A planar homography estimation method for camera calibration. In *Proceedings 2003 IEEE International Symposium on Computational Intelligence in Robotics and Automation*, volume 1, pages 424–429, July 2003. 1
- [6] Paolo Galeone. Camera calibration guidelines, 2018. <https://pgaleone.eu/computer-vision/2018/03/04/camera-calibration-guidelines/>. 1
- [7] Etienne Grossmann, John Iselin Woodfill, and Gaile Gibson Gordon. Camera calibration using an easily produced 3D calibration pattern, Oct. 2014. 1
- [8] Erwan Guillou, Daniel Meneveau, Eric Maisel, and Kadi Bouatouch. Using vanishing points for camera calibration and coarse 3d reconstruction from a single image. *The Visual Computer*, 16(7):396–410, 2000. 1
- [9] Daniel Herrera, C. Juho Kannala, and Janne Heikkila. Forget the checkerboard: Practical self-calibration using a planar scene. In *2016 IEEE Winter Conference on Applications of Computer Vision (WACV)*, pages 1–9, Lake Placid, NY, USA, Mar. 2016. IEEE. 1
- [10] Lin Huang, Feipeng Da, and Shaoyan Gai. Research on multi-camera calibration and point cloud correction method based on three-dimensional calibration object. *Optics and Lasers in Engineering*, 115:32–41, Apr. 2019. 1
- [11] J. Kannala and S.S. Brandt. A generic camera model and calibration method for conventional, wide-angle, and fish-eye lenses. *IEEE Transactions on Pattern Analysis and Machine Intelligence*, 28(8):1335–1340, Aug. 2006. 2, 3
- [12] Jana Košecká and Wei Zhang. Video Compass. In *European conference on computer vision*, Lecture Notes in Computer Science, pages 476–490, Berlin, Heidelberg, 2002. Springer. 1, 6
- [13] Joo-Haeng Lee. Camera calibration from a single image based on coupled line cameras and rectangle constraint. In *Pattern Recognition (ICPR), 2012 21st International Conference on*, pages 758–762. IEEE, 2012. 1
- [14] Vincent Lepetit, Francesc Moreno-Noguer, and Pascal Fua. EPnP: An Accurate O(n) Solution to the PnP Problem. *International Journal of Computer Vision*, 81(2):155, July 2008. 7
- [15] Xiaoyu Li, Bo Zhang, Pedro V. Sander, and Jing Liao. Blind geometric distortion correction on images through deep learning. In *IEEE Conf. Comput. Vis. Pattern Recog.*, May 2019. 1
- [16] Kang Liao, Chunyu Lin, and Yao Zhao. A Deep Ordinal Distortion Estimation Approach for Distortion Rectification. *arXiv:2007.10689 [cs]*, July 2020. arXiv: 2007.10689. 1
- [17] Yaowen Lv, Wei Liu, and Xiping Xu. Methods based on 1D homography for camera calibration with 1D objects. *Applied Optics*, 57(9):2155–2164, Mar. 2018. 1
- [18] Jorge J. Moré. *The Levenberg-Marquardt algorithm: Implementation and theory*. Lecture Notes in Mathematics. Springer, Berlin, Heidelberg, 1978. 6
- [19] PanoTools. Fisheye Projection. https://wiki.panotools.org/Fisheye_Projection, 2020. 3
- [20] Klaus H. Strobl and Gerd Hirzinger. More accurate pinhole camera calibration with imperfect planar target. In *2011 IEEE International Conference on Computer Vision Workshops (ICCV Workshops)*, pages 1068–1075, Barcelona, Spain, Nov. 2011. IEEE. 1
- [21] John Wallis. *A Treatise of Algebra, Both Historical and Practica*. Oxford: Richard Davis, 1685. 4
- [22] Wikipedia. Fisheye lens. https://en.wikipedia.org/w/index.php?title=Fisheye_lens&oldid=986382882. 3
- [23] Zhucun Xue, Nan Xue, Gui-Song Xia, and Weiming Shen. Learning to Calibrate Straight Lines for Fisheye Image Rectification. In *IEEE Conf. Comput. Vis. Pattern Recog.*, May 2019. 1
- [24] Zhu-Cun Xue, Nan Xue, and Gui-Song Xia. Fish-eye Distortion Rectification from Deep Straight Lines. *arXiv:2003.11386 [cs]*, Mar. 2020. arXiv: 2003.11386. 1
- [25] Xiaoqing Yin, Xinchao Wang, Jun Yu, Maojun Zhang, Pascal Fua, and Dacheng Tao. Fisheyecnet: A multi-context collaborative deep network for fisheye image rectification. In *Eur. Conf. Comput. Vis.*, May 2018. 1
- [26] Beiwei Zhang and Youfu Li. Homography-based method for calibrating an omnidirectional vision system. *Journal of the Optical Society of America A*, 25(6):1389–1394, June 2008. 1
- [27] Zhengyou Zhang. A flexible new technique for camera calibration. *IEEE Transactions on pattern analysis and machine intelligence*, 22(11):1330–1334, Nov. 2000. 2, 5, 6, 7
- [28] H. Zhao, Y. Shi, X. Tong, X. Ying, and H. Zha. A Simple Yet Effective Pipeline For Radial Distortion Correction. In *2020 IEEE International Conference on Image Processing (ICIP)*, pages 878–882, Oct. 2020. ISSN: 2381-8549. 1
- [29] Zhengyou Zhang. Flexible camera calibration by viewing a plane from unknown orientations. In *Proceedings of the Seventh IEEE International Conference on Computer Vision*, pages 666–673 vol.1, Kerkyra, Greece, 1999. IEEE. 1